NON-LINEAR HOMOGENIZATION THEORIES WITH APPLICATIONS TO TRIP STEELS

I. Papadioti[1], I. Bellas[1], M-I.T. Tzini[1], P.I. Christodoulou[1] and N. Aravas[1,2]

[1]Department of Mechanical Engineering
University of Thessaly
Volos, GR-38334, Greece
e-mail: papadioti@uth.gr, iliasbellas@gmail.com, margiannatz@gmail.com, pchristod@uth.gr, aravas@uth.gr

[2]International Institute for Carbon Neutral Energy Research (WPI-I2CNER)
Kyushu University
Fukuoka 819-0395, Japan

Keywords: Homogenization; Elasto-plasticity; Composite materials; Finite strains; TRIP steels.

Abstract. *A general constitutive model for N−phase isotropic, incompressible, rate-independent elasto-plastic composite materials at finite strains is developed. The formulation is based on the non-linear homogenization variational (or modified secant) method which makes use of a linear comparison composite (LCC) material to estimate the effective flow stress of the non-linear composite material. The homogenization approach leads to an algebraic optimization problem, which for a two-phase material* $(N=2)$ *is solved analytically, whereas for* $N \geq 3$ *the solution is obtained numerically. The model is validated by periodic three-dimensional unit cell calculations comprising a large number of spherical inclusions distributed randomly in a matrix phase. The homogenization technique provides accurate estimates not only for the effective flow stress but also for the average strains in the constituent phases. These estimates form the basis for the development of an approximate analytical model for the elastoplastic behavior of a composite with hardening phases. The predictions of the model are in excellent agreement with the results of detailed unit cell finite element calculations of a composite with hardening phases for different types of loadings, including uniaxial tension and finite shear. The homogenization theory is also used to develop a constitutive model for the mechanical behavior of* ***TRIP*** *(**TR**ansformation **I**nduced **P**lasticity) steels. TRIP steels are essentially composite materials with evolving volume fractions of the constituent phases. The calibration of the model is based on uniaxial tension tests on TRIP steels. The constitutive model is used for the calculation of "**F**orming **L**imit **D**iagrams" (FLDs) for sheets made of TRIP steels; it is found that the TRIP phenomenon increases the strain at which local necking results from a gradual localization of the strains at an initial thickness imperfection in the sheet.*

1 INTRODUCTION

An analytical and numerical methodology for estimation of the effective response of N-phase isotropic elasto-plastic metallic composites is developed. Special attention is given to particulate microstructures, i.e., composite materials with a distinct matrix phase and an isotropic distribution of spherical particles. The particles are assumed to be stiffer than the matrix, which is the case in most metallic materials of interest, such as TRIP steels. Such materials, usually contain second-phase particles (e.g., intermetallics, carbon particles) or just second and third phase variants (e.g., retained austenite, bainite, martensitic phases). In addition, these phases/particles tend to reinforce the yield strength of the composite while they usually have different strength and hardening behavior than the host matrix phase.

In the literature of non-linear homogenization there exists a large number of studies for two-phase composite materials. Nonetheless, very few studies exist in the context of three- or N-phase composites. In view of this, the present work uses the non-linear variational homogenization method of Ponte Castañeda [1], which makes use of a linear comparison composite (LCC) material, to estimate the effective response of a N-phase non-linear composite material. Simple analytical expressions are given for the effective yield stress of a two-phase composite (see also Ponte Castañeda and deBotton [2]) while a simple semi-analytical expression (requiring the solution of a constrained optimization problem for $N-1$ scalar quantities) is given for the $N-$phase composite. Additional analytical expressions are also provided for the phase concentration tensors and average strains in each phase in terms of the aforementioned optimized scalar quantities.

2 THE HOMOGENIZATION METHOD

We consider a composite material made of N isotropic, incompressible viscoplastic phases. The phases are distributed randomly and isotropically. The constitutive equations of each phase is of the form:

$$\mathbf{D}=\frac{\partial U}{\partial \boldsymbol{\sigma}}=\dot{\bar{\varepsilon}}\,\mathbf{N},\quad U\left(\sigma_e\right)=\frac{\sigma_0\,\dot{\varepsilon}_0}{n+1}\left(\frac{\sigma_e}{\sigma_0}\right)^{n+1},\quad \text{with}\quad \dot{\bar{\varepsilon}}=\dot{\varepsilon}_0\left(\frac{\sigma_e}{\sigma_0}\right)^{n},\quad \mathbf{N}=\frac{\partial \sigma_e}{\partial \boldsymbol{\sigma}}=\frac{3}{2\sigma_e}\mathbf{s}, \tag{1}$$

where $\mathbf{D}$ is the deformation rate, $\boldsymbol{\sigma}$ the stress tensor, $p=\sigma_{kk}/3$ the hydrostatic stress, $\mathbf{s}=\boldsymbol{\sigma}-p\boldsymbol{\delta}$ the stress deviator, $\boldsymbol{\delta}$ being the second-order identity tensor, $\sigma_e=\sqrt{\frac{3}{2}\mathbf{s}:\mathbf{s}}$ the von Mises equivalent stress, σ_0 is a reference stress, $\dot{\varepsilon}_0$ a reference strain rate, n the creep exponent $\left(1\le n\le\infty\right)$, $\mathbf{N}$ is a second order tensor that defines the direction of $\mathbf{D}$ and $\dot{\bar{\varepsilon}}=\sqrt{\frac{2}{3}\mathbf{D}:\mathbf{D}}$ is the equivalent plastic strain rate that defines the magnitude of $\mathbf{D}$.

The constitutive equation of the isotropic non-linear composite is written in terms of the effective viscoplastic stress potential $\tilde{U}\left(\boldsymbol{\sigma}\right)$ so that

$$\mathbf{D}=\frac{\partial \tilde{U}}{\partial \boldsymbol{\sigma}}, \tag{2}$$

where $\boldsymbol{\sigma}$ and $\mathbf{D}$ are respectively the macroscopic stress and deformation rate in the composite. An estimate for $\tilde{U}$ is obtained by using the variational methodology of Ponte Castañeda ([1], [3]):

$$\tilde{U}\left(\sigma_e\right)=\sup_{\mu^{(r)}\ge 0}\left\{\frac{\sigma_e^2}{6\tilde{\mu}\left(\mu^{(r)}\right)}-\sup_{\sigma_e^{(r)}\ge 0}\sum_{r=1}^{N}c^{(r)}\left[\frac{\left(\sigma_e^{(r)}\right)^2}{6\,\mu^{(r)}}-U^{(r)}\left(\sigma_e^{(r)}\right)\right]\right\}, \tag{3}$$

where $\tilde{\mu}$ is the effective viscosity of the "linear comparison composite" (LCC). One way to estimate $\tilde{\mu}$ is to use the well-known Hashin-Shtrikman relationship for particulate composites [4].

An approximation for the deformation rate field in the non-linear composite may be obtained from the deformation rate field in the LCC evaluated at the optimal comparison moduli $\hat{\mu}^{(r)}$ defined by the optimization problem in (3). In particular, the average deformation rate field in the phases $\mathbf{D}^{(r)}$ may be determined from the macroscopic deformation rate $\mathbf{D}$ in terms of a "strain concentration tensor" $\mathbf{A}^{(r)}$

$$\mathbf{D}^{(r)}=\mathbf{A}^{(r)}:\mathbf{D}\,, \tag{4}$$

where

$$\mathbf{D}^{(r)}=\mathbf{A}^{(r)}:\mathbf{D}=a^{(r)}\,\mathbf{D},\qquad a^{(r)}=\frac{1}{3\mu_0+2\hat{\mu}^{(r)}}\left(\sum_{s=1}^{N}\frac{c^{(s)}}{3\mu_0+2\hat{\mu}^{(s)}}\right)^{-1}, \tag{5}$$

$c^{(r)}$ are the volume fractions of the phases and μ_0 a reference viscosity. Details of the derivation are given in Papadioti *et al*. [5].

2.1 Perfectly Plastic Phases

We consider the case of perfectly plastic phases $(n^{(r)}\to\infty)$. The optimization in (3) as $(n^{(r)}\to\infty)$ is carried out in three steps. In the first step, we consider the optimization over $\sigma_e^{(r)}$. All creep exponents are set equal in the second step, i.e., we set $n^{(1)}=n^{(2)}=\cdots=n^{(N)}\equiv n$. In the final third step we consider the limit $n^{(r)}\to\infty$. Details of the derivation are given in Papadioti *et al*. [5].

The resulting effective potential $\tilde{U}(\sigma_e)$ defines the effective flow stress $\tilde{\sigma}_0$ of the composite:

$$\tilde{\sigma}_0 = \sqrt{\inf_{\substack{y^{(1)}=1,\, y^{(r)}\geq 0 \\ i=2,\ldots,N}} \frac{H_\infty\left(y^{(r)}\right)}{F\left(y^{(r)}\right)}},$$
$$H_\infty\left(y^{(r)}\right) = \sum_{r=1}^{N} c^{(r)}\left(\sigma_0^{(r)}\right)^2 y^{(r)}, \qquad F\left(y^{(r)}\right) = \left(\sum_{r=1}^{N} \frac{c^{(r)}\, y^{(r)}}{3y^{(r)}+2y_0}\right)\left(\sum_{s=1}^{N} \frac{c^{(s)}}{3y^{(s)}+2y_0}\right)^{-1}, \tag{6}$$

where $y^{(r)} = \mu^{(1)} / \mu^{(r)}$ and $y_0 = \mu^{(1)} / \mu_0$.

Calculation of the effective yield stress $\tilde{\sigma}_0$ requires the solution of the constrained optimization problem in (6) for the values of $y^{(r)}$, which define in turn the appropriate values of the viscosities $\mu^{(r)}$. In the special case of a two-phase composite $(N=2)$ the solution of the optimization problem can be found analytically as described in Section 2.2. The solution of more general cases $(N \geq 3)$ is obtained by using the methodology of Kaufman *et al*. [6] and the CONMAX software for the solution of the optimization problem in (6).

The strain concentration values $a^{(r)}$ defined in (5) can be written in the form

$$a^{(r)} = \frac{\hat{y}^{(r)}}{3\hat{y}^{(r)}+2y_0}\left(\sum_{s=1}^{N} \frac{c^{(s)}\hat{y}^{(s)}}{3\hat{y}^{(s)}+2y_0}\right)^{-1}, \tag{7}$$

where $\hat{y}^{(r)}$ are the optimal values of $y^{(r)}$ resulting from the optimization in (6).

2.2 The two-phase perfectly plastic composite – An analytic estimate for the effective flow stress and the strain concentration factors

We consider an isotropic two-phase composite $(N=2,\ c^{(1)}+c^{(2)}=1)$. Each phase is perfectly plastic with flow stress $\sigma_0^{(1)}$ and $\sigma_0^{(2)}$. The estimate for $\tilde{\sigma}_0$ depends on the chosen value of the reference viscosity μ_0. Results for various choices of μ_0 are reported in Papadioti [7]. Here we present in some detail the formulation based on a Hashin-Strikman lower bound with $\mu_0 = \mu^{(1)}$ $(y_0 = 1)$; this particular choice of μ_0 shows the best agreement with detailed unit cell finite element calculations.

For $\mu_0 = \mu^{(1)}$, the ratio H_∞ / F in (6) takes the value

$$\frac{H_\infty\left(y^{(2)}\right)}{F\left(y^{(2)}\right)} = \left(\sigma_0^{(1)}\right)^2\left(c^{(1)}+c^{(2)}r^2\, y^{(2)}\right)\frac{2+3c^{(2)}+3c^{(1)}\, y^{(2)}}{2c^{(1)}+\left(3+2c^{(2)}\right)y^{(2)}}, \qquad r=\frac{\sigma_0^{(2)}}{\sigma_0^{(1)}}>1. \tag{8}$$

The optimum value of $\hat{y}^{(2)}$ to be used in (6) is calculated by using the condition

$$\frac{\partial}{\partial y^{(2)}}\left(\frac{H_\infty}{F}\right) = 0 \tag{9}$$

together with the constraint $y^{(2)} \geq 0$. After some lengthy, but straightforward, calculations we find the resulting optimal value $\hat{y}^{(2)}$ to be

$$\hat{y}^{(2)} = \begin{cases} \dfrac{1}{3+2c^{(2)}}\left[-2c^{(1)} + \dfrac{5}{\sqrt{3}}\sqrt{\left(3+2c^{(2)}\right)\dfrac{1}{r^2} - 2c^{(2)}}\right] & \text{if} \quad 1 \leq r \leq r_{\text{cr}} \quad \left(c^{(2)} \leq c_{\text{cr}}^{(2)}\right), \\ 0 & \text{if} \quad r \geq r_{\text{cr}} \quad \left(c^{(2)} \geq c_{\text{cr}}^{(2)}\right), \end{cases} \tag{10}$$

where

$$r_{\rm cr} = \frac{5}{\sqrt{4+6c^{(2)}}} \qquad \text{and} \qquad c_{\rm cr}^{(2)} = \frac{1}{6}\left[\left(\frac{5}{r}\right)^2 - 4\right]. \tag{11}$$

According to (10), for a given particle concentration $c^{(2)}$, when the contrast ratio $r = \sigma_0^{(2)} / \sigma_0^{(1)}$ is larger than a value r_{cr}, the comparison material for phase 2 is rigid $\left(\hat{y}^{(2)} = 0\right)$.

The corresponding estimate for the effective flow stress resulting from (6) is

$$\frac{\tilde{\sigma}_0}{\sigma_0^{(1)}} = \begin{cases} \dfrac{1}{3+2c^{(2)}}\left[5c^{(2)}\, r + c^{(1)}\sqrt{9+6c^{(2)}\left(1-r^2\right)}\right] & \text{if} \quad 1 \le r \le r_{\rm cr} \quad \left(c^{(2)} \le c_{\rm cr}^{(2)}\right), \\ \dfrac{1}{2}\sqrt{4+6c^{(2)}} & \text{if} \quad r_{\rm cr} \le r \qquad \left(c_{\rm cr}^{(2)} \le c^{(2)}\right). \end{cases} \tag{12}$$

The strain concentration values $a^{(r)}$ given in (7) can be written in the form

$$a^{(1)} = \frac{1}{\left(2y_0+3\right)\mathcal{D}}, \qquad a^{(2)} = \frac{\hat{y}^{(2)}}{\left(2y_0+3\hat{y}^{(2)}\right)\mathcal{D}}, \qquad \mathcal{D} = \frac{c^{(1)}}{2y_0+3} + \frac{c^{(2)}\,\hat{y}^{(2)}}{2y_0+3\hat{y}^{(2)}} \tag{13}$$

and $\hat{y}^{(2)}$ is defined in (10).

3 UNIT CELL FINITE ELEMENT CALCULATIONS AND ASSESSMENT OF THE MODEL

In this section we present the results of unit cell finite element calculations for a composite material made up of a statistically isotropic random distribution of isotropic, linearly-elastic perfectly-plastic spherical inclusions embedded in a continuous, isotropic, linearly-elastic perfectly-plastic matrix. The elastic Young modulus used in the finite element calculations for all phases is three orders of magnitude higher than the highest yield stress involved; this minimizes the effects of elasticity and the results are very close to those of rigid-perfectly-plastic materials.

We study numerically two- and three-phase composites. The matrix is labelled as phase 1 and the reinforcing particles are spherical and have higher flow stresses $\left(\sigma_0^{(i)} > \sigma_0^{(1)}, \quad i > 1\right)$. The periodic unit cell is a cube with edge size L and is constructed using the method presented by Segurado and Llorca [8] and extended to polydisperse inclusion distributions by Lopez-Pamies *et al.* [9]. The virtual microstructure contains a dispersion of a sufficiently large number of non-overlapping spheres of uniform (monodisperse) or different (polydisperse) size. The inclusions are randomly located within the cell and are generated using the Random Sequential Adsorption Algorithm (RSA) [10].

3.1 The effective yield stress

We determine numerically the effective yield stress by solving the problem of a unit cell loaded in uniaxial tension. Figure 1a shows the variation of the calculated effective flow stress from the unit cell finite element calculations with the contrast ratio $r = \sigma_0^{(2)} / \sigma_0^{(1)}$ for various volume fractions, together with the predictions (6) of the homogenization model, based on the Hashin-Shtrikman lower bound $\left(\mu_0 = \mu^{(1)}\right)$. For that data shown in Fig. 1a, the maximum difference between the predictions (6) and the results of the unit cell finite element calculations is 3%. It is also interesting to mention that an increase of the flow stress $\sigma_0^{(2)}$ in the inclusions beyond (approximately) two times the flow stress of the matrix $\left(2\sigma_0^{(1)}\right)$ does not change the effective flow stress of the composite for all volume fractions considered here. Figure 1b shows the variation of $\tilde{\sigma}_0 / \sigma_0^{(1)}$ of a three-phase composite for different values of the volume fraction $c^{(3)}$ as determined from the unit cell finite element calculations and the predictions (6) of the homogenization model. The material data are typical for a TRIP steel with a ferritic matrix (phase 1) containing retained austenite (phase 2), which transforms gradually to martensite

(phase 3) as the TRIP steel deforms plastically.

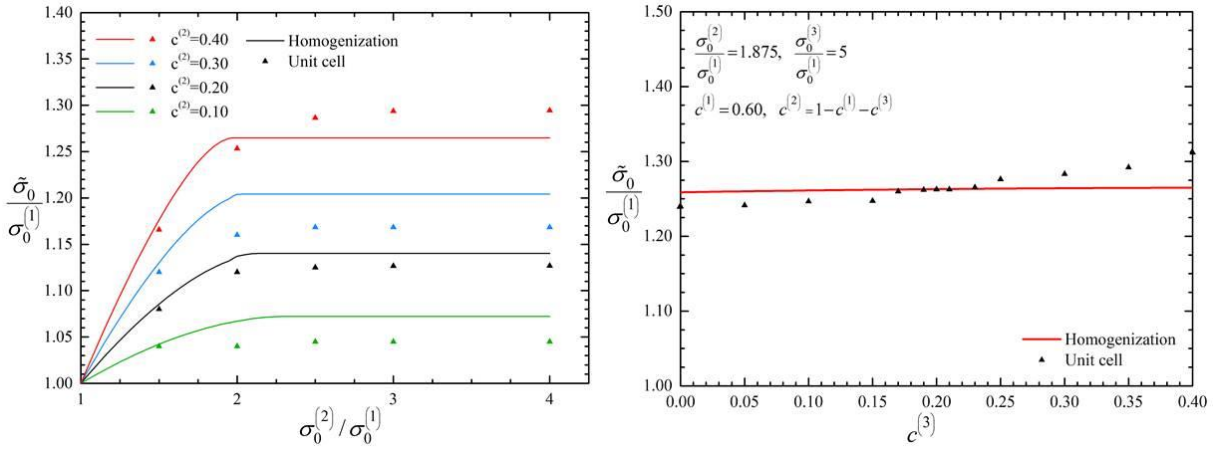

Figure 1. Variation of normalized effective flow stress $\tilde{\sigma}_0 / \sigma_0^{(1)}$ (a) of a two-phase composite for various volume fractions (b) of a three-phase composite for different values of the volume fraction $c^{(3)}$.

3.2 The strain concentration tensors

The unit cell finite element calculations discussed above were used also to determine the strain concentration factors defined in (7). Figure 2a shows the variation of the strain concentration factors $a^{(r)}$ in a two-phase composite with the contrast ratio $r = \sigma_0^{(2)} / \sigma_0^{(1)}$ for $c^{(2)} = 0.30$ as determined from the unit cell finite element calculations and the homogenization theory. An important observation in the context of this figure is that at a contrast ratio of $r \simeq 2$, a sharp transition is observed where the particles start behaving as being rigid, i.e., the average strain in the particle is almost zero. This is validated by both the model and the numerical results. A similar plot for a three-phase composite is shown in Fig. 2b. The predictions of homogenization theory agree well with the results of the unit cell finite element calculations.

3.3 On the possible dependence of the effective flow stress on J_3

Suquet and Ponte Castañeda [11],[12] studied the effective mechanical behavior of weakly inhomogeneous composites and showed that, for the case of incompressible "power-law" phases, the effective potential of the composite may depend, to second order, on the third invariant of the applied strain.

We carry out detailed unit cell finite element calculations in order to check for a possible dependence of the effective yield stress $\tilde{\sigma}_0$ on the third invariant J_3 of the stress deviator $\mathbf{s}$ ($J_3 = \det \mathbf{s} = -\left(2/27\right)\sigma_e^3 \sin 3\theta$, where θ is the "Lode angle"). Angle θ takes values in the range $-30^\circ \le \theta \le 30^\circ$, where, to within a given hydrostatic stress, $\theta = -30^\circ$ corresponds to uniaxial tension, $\theta = 0^\circ$ to pure shear, and $\theta = 30^\circ$ to uniaxial compression.

Figure 3 illustrates the variation of the normalized effective flow stress $\tilde{\sigma}_0 / \sigma_0^{(1)}$ as determined from unit cell finite element calculations, with Lode angle θ for particle volume fractions $c^{(2)} = 0.10$, 0.20 and 0.40. It is shown that the effective flow stress of the composite is essentially independent of the third stress invariant J_3 which is in agreement with earlier results by Idiart [13] in the case of rigid particles.

4 HARDENING PHASES

In this section we present an approximate method for the prediction of the incremental elastoplastic behavior of macroscopically isotropic composites made of N isotropic, rate-independent, elastic-plastic hardening phases. Let the flow stresses $\sigma_y^{(i)}$ of each phase be known functions of the corresponding equivalent plastic strains $\bar{\varepsilon}^{(i)}$ $(i = 1, 2, \ldots, N)$.

It should be noted that the elastic and plastic response of the homogenized composite are treated independently, and combined later to obtain the full elastic-plastic response. The composite is assumed to behave as "incrementally perfectly plastic" with a flow stress $\tilde{\sigma}_0$, which is updated at every increment. The value of $\tilde{\sigma}_0$

is calculated by the solution of the corresponding optimization problem (6) using the $\sigma_0^{(i)}$ values at each increment. The solution of the optimization problem (6) defines also the optimal values $\hat{y}^{(i)}$, which determine the corresponding strain concentration factors $a^{(i)}$ in (7) for the increment. Details on the numerical integration of constitutive equations are given in Papadioti [7].

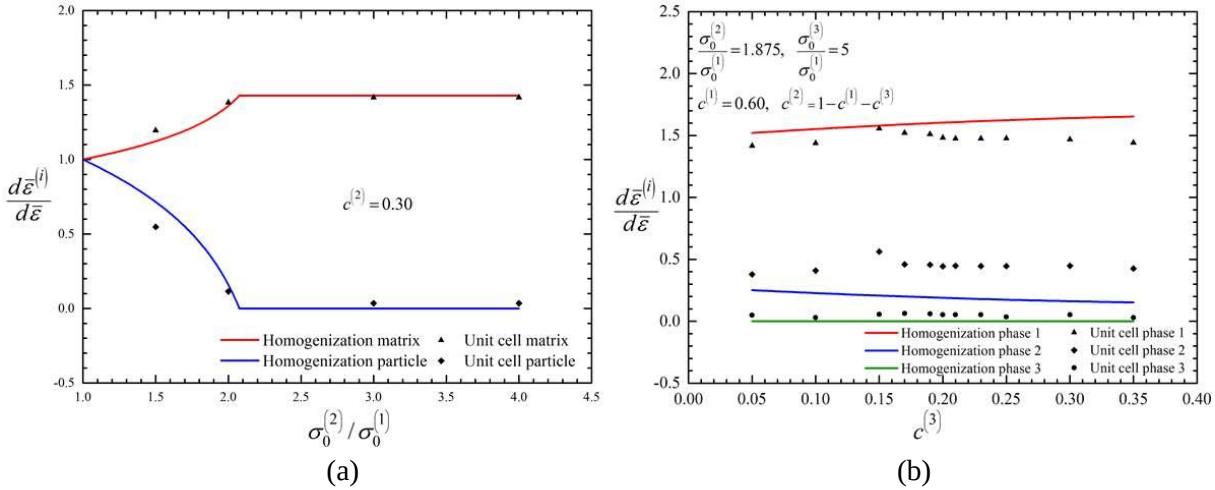

(a) (b)

Figure 2. Strain concentration factors $a^{(r)}$ (a) for a two-phase composite and (b) for a three-phase composite.

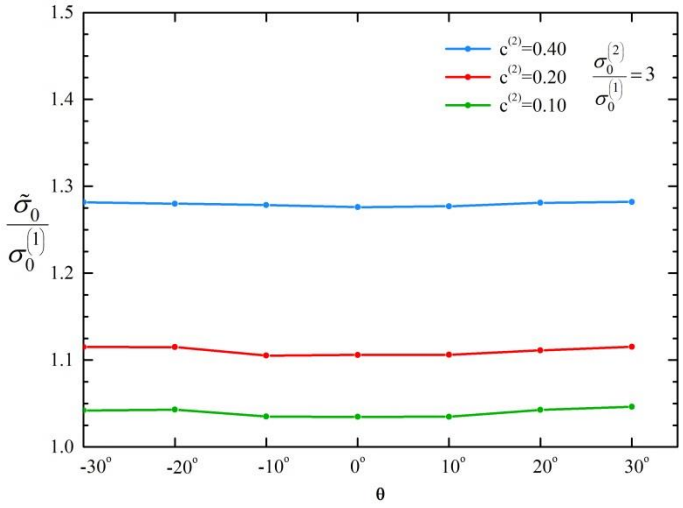

Figure 3. Variation of effective normalized flow stress $\tilde{\sigma}_0 / \sigma_0^{(1)}$ with Lode angle θ for particle volume fractions of 10, 20 and 40%. The results show almost no dependence on J_3.

4.1 Unit cell calculations and assessment of the model with hardening phases

In this section we present the results of unit cell finite element calculations for a composite material made up of a statistically isotropic random distribution of isotropic, linearly-elastic hardening-plastic spherical inclusions embedded in a continuous, isotropic, linearly-elastic hardening-plastic matrix. All analyses were carried out incrementally and accounted for geometry changes due to deformation (finite strain solutions).

In all cases analyzed, the matrix material is identified as "phase 1" and the flow stress $\sigma_y^{(i)}$ of "phase i" is a function of the corresponding equivalent plastic strain $\bar{\varepsilon}^{(i)}$:

$$\sigma_y^{(i)}\left(\bar{\varepsilon}^{(i)}\right)=\sigma_0^{(i)}\left(1+\frac{\bar{\varepsilon}^{(i)}}{\varepsilon_0}\right)^{\frac{1}{\eta^{(i)}}}, \qquad \varepsilon_0=0.005, \tag{14}$$

where $\sigma_0^{(i)}$ is the yield stress of phase i, E is the elastic Young's modulus, and the hardening exponents $\eta^{(i)}$ take values in the region $1\le\eta^{(i)}\le\infty$, with the limiting case $\eta^{(i)}=\infty$ corresponding to perfect plasticity. The values $E=917\sigma_0^{(1)}$ and $\nu=0.3$ for Young's modulus E and Poisson ratio ν are used in the calculations.

In addition, one-element finite element calculations were carried out, in which the element is subjected to the same deformation gradient as the unit cell and the corresponding uniform stress state in the element is calculated for the homogenized material. In particular, we consider a three-phase composite with

$$\frac{\sigma_0^{(2)}}{\sigma_0^{(1)}}=1.875, \quad \frac{\sigma_0^{(3)}}{\sigma_0^{(1)}}=5, \quad \eta^{(1)}=5, \quad \eta^{(2)}=3, \quad \eta^{(3)}=2.5. \tag{15}$$

The problems of uniaxial tension and finite shear deformation are solved. Figure 4 shows the deformed unit cells for uniaxial tension at $\lambda=1.20$ and finite shear $\gamma=0.20$ and Figure 5 shows the stress-strain curves in uniaxial tension and finite shear, for a three-phase composite with composition $c^{(1)}=0.60$, $c^{(2)}=0.25$, and $c^{(3)}=0.15$. The predictions of the homogenization model agree well with the results of the unit cell finite element calculations. The model is capable of predicting sufficiently well both the initial yield strength of the three-phase composite as well the hardening evolution as a function of the applied strains both in uniaxial tension and shear loadings.

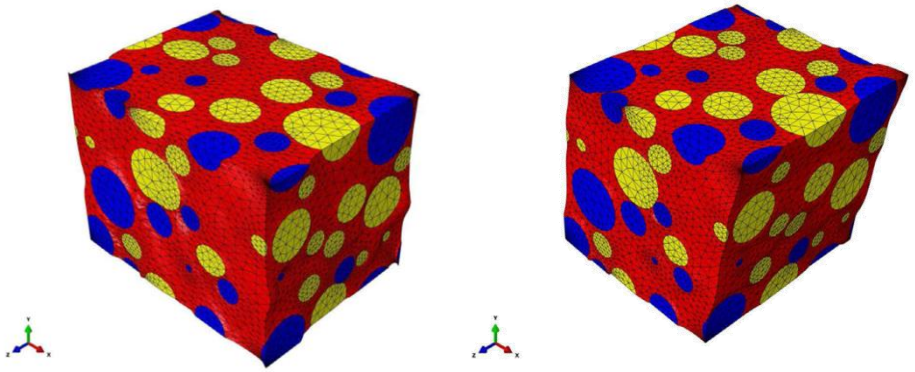

Figure 4. Deformed configurations of unit cells of the three-phase composite in uniaxial tension and simple shear.

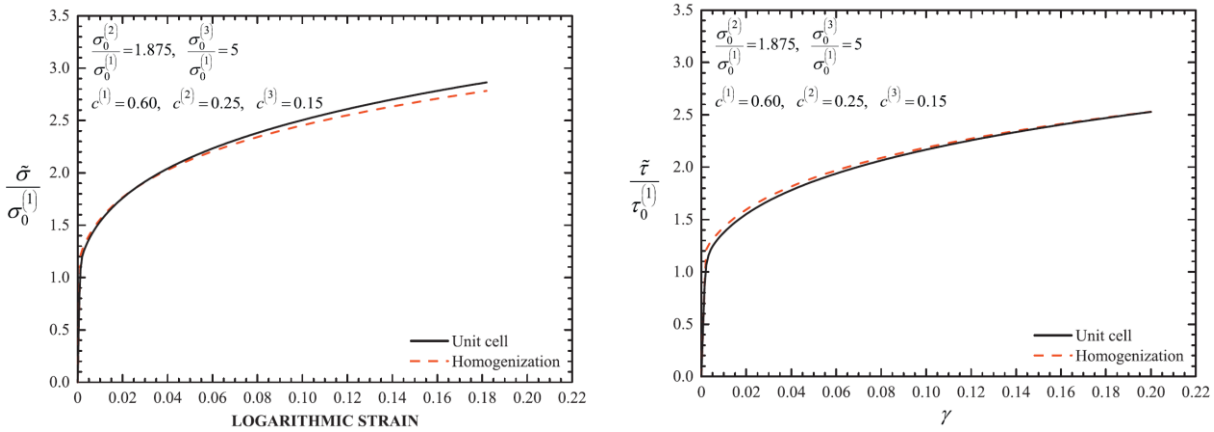

Figure 5 Stress-strain curves of the three-phase composite in uniaxial tension and simple shear.

5 APPLICATIONS TO TRIP STEELS

The homogenization techniques for non-linear composites, described in the previous sections, are used to

determine the effective properties and overall behavior of TRIP steels. We consider four-phase TRIP steels that consist of a ferritic matrix with dispersed bainite and austenite, which transforms gradually into martensite as the material deforms plastically. The following labels are used for the constituent phases: (1) for ferrite, (2) for bainite, (3) or (a) for austenite and (4) or (m) for martensite. The constitutive equations are developed for the case of finite geometry changes.

An important aspect of the martensitic transformation is the strain softening which occurs due to the strain associated with the transformation process. This strain softening is accounted for by introducing in the constitutive model an additional deformation rate that is proportional to the rate of increase of the volume fraction of martensite. The total deformation rate can be split into elastic, plastic and transformation parts:

$$\mathbf{D} = \mathbf{D}^e + \mathbf{D}^p + \mathbf{D}^{TRIP} . \tag{16}$$

Details on the constitutive formulation and the numerical integration of the resulting elastoplastic constitutive equations are given in Papadioti [7]. The model is then implemented into the ABAQUS. The calibration of the model is based on experimental data of uniaxial tension tests on TRIP. The constitutive model is also used to calculate "forming limit diagrams" for sheets made of TRIP steels. Calculations are also conducted for a non-transforming steel for comparison purposes.

5.1 Forming Limit Diagrams

In this section, the constitutive model developed for the four-phase TRIP steel is used to calculate "forming limit diagrams" for sheets made of TRIP steels. Forming limit diagrams show the maximum deformation to which a sheet metal can be subjected before the material fails. In the present work, we concentrate on the formation of instabilities in a narrow straight band in metal sheets deformed under plane stress conditions. The predictions of the analytical model are compared to experimental data from the same TRIP steel which was used for the calibration. For comparison purposes, a separate set of calculations is conducted for a non-transforming TRIP steel with same initial values of the volume fractions of the phases.

We consider a sheet made of TRIP steel that is deformed uniformly on its plane in a way that the in-plane principal strain increments increase proportionally. We study the possibility of the formation of an instability in the form of a narrow straight band and construct the corresponding ''forming limit diagram''.

We follow the approach of Marciniak and Kuzynski [14], known as the ''M–K'' model, in which the sheet is assumed to contain a small initial inhomogeneity and necking results from a gradual localization of the strains at the inhomogeneity. The inhomogeneity is in the form of straight narrow band (neck) of reduced thickness $H^b < H$. Both inside and outside the band a state of uniform plane stress is assumed, and the analysis consists in determining the uniform state of deformation inside the band that is consistent kinematically and statically with the prescribed uniform state outside the band. Given the initial sheet thickness inside and outside the band and the imposed uniform deformation history outside the band, the equations of equilibrium are solved incrementally to obtain the deformation history inside the band. Localization is said to occur when the ratio of some scalar measure of the amount of incremental straining inside the band to the corresponding value outside the band becomes unbounded.

The initial volume fractions of the four phases in the TRIP steel are assumed to be $c^{(1)} = 0.50$, $c^{(2)} = 0.38$, $c^{(a)} = 0.103$ and $c^{(m)} = 0.017$. The curves $\sigma_y^{(r)}, r = 1,4$ that define the variation of the flow stress of the phases are (in MPa):

$$\begin{aligned} \sigma_y^{(1)} &= 260\left(1+\frac{\bar{\varepsilon}}{0.0042}\right)^{\frac{1}{4.25}}, \quad \sigma_y^{(a)} = 550\left(1+\frac{\bar{\varepsilon}}{0.1}\right)^{\frac{1}{4.2}}, \\ \sigma_y^{(2)} &= 825\left(1+\frac{\bar{\varepsilon}}{0.0104}\right)^{\frac{1}{10.36}}, \quad \sigma_y^{(m)} = 1132\left(1+\frac{\bar{\varepsilon}}{0.0004}\right)^{\frac{1}{16.65}}. \end{aligned} \tag{17}$$

Figure 6 illustrates forming limit curves obtained for imposed proportional straining ρ for two different values of the initial thickness imperfection, namely $H^b/H = 0.999$ and $H^b/H = 0.99$ and for the case without imperfection i.e. $H^b/H = 1$. The three solid curves correspond to the TRIP steel, whereas the dashed curves are for the non-transforming steel. As we can see, the TRIP effect increases the necking localization strains. This result was also presented by Papatriantafillou *et al.* [15], who used a rate dependent constitutive model for TRIP steels (as opposed to the rate independent model used here). In details, for no imperfection and $\rho = 0$ (plane

strain), the critical strain ε_{11}^{cr} increases from 0.19228 for the non-transforming steel to 0.21203 for the TRIP steel; the corresponding values of ε_{11}^{cr} for $H^b/H = 0.999$ and $\rho = 0$ are 0.17369 for the non-transforming steel and 0.19395 for the TRIP steel and for $H^b/H = 0.99$ and $\rho = 0$ are 0.13775 for the non-transforming steel and 0.15869 for the TRIP steel.

The model predictions are also compared to available experimental data. The experimental data refer to the same TRIP steel which was used for the calibration of the model. Details on the experiments are given in Papatriantafillou et al. [15]. The model predictions fit the experimental data reasonably well.

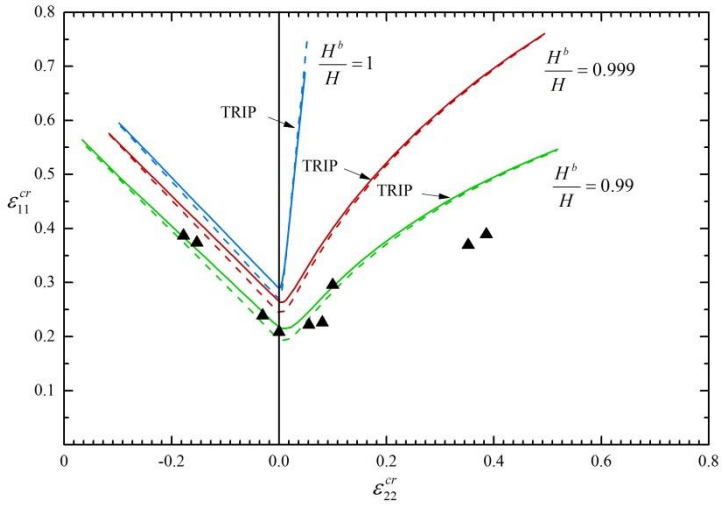

Figure 6 Forming limit curves for two different values of initial thickness inhomogeneities $H^b/H = 0.999$ and $H^b/H = 0.99$. The solid lines correspond to the TRIP steel, whereas the dashed lines are for a non-transforming steel. The dark triangles are experimental data.

6 ACKNOWLEDGEMENTS

This work was carried out in the framework of “TRIP steels: Simulation and experimental study of heat treatment and mechanical behavior” project. This research is implemented through the Operational Program "Human Resources Development, Education and Lifelong Learning" and is co-financed by the European Union (European Social Fund) and Greek national funds. The authors would like also to acknowledge the help of late Prof. A. Stamatis of University of Thessaly on the solution of the optimization problem. Use of the FORTRAN code CONMAX (http://www.netlib.org/opt/conmax.f) is gratefully acknowledged.

REFERENCES

[1] Ponte Castañeda P. (1991), "The effective mechanical properties of non-linear isotropic composites", J. Mech. Phys. Solids Vol. 39, pp. 45-71.

[2] Ponte Castañeda P. and deBotton G. (1992), "On the homogenized yield strength of two-phase composites", Proc. R. Soc. Lond. A Vol. 438, pp. 419-431.

[3] Ponte Castañeda P. (1992), "New variational principles in plasticity and their application to composite materials", J. Mech. Phys. Solids Vol. 40, pp. 1757-1788.

[4] Willis J.R. (1982), "Elasticity theory of composites" In: Hopkins H.G., Sewell M.J. (Eds.), Mechanics of Solids, The Rodney Hill 60th Anniversary Volume. Pergamon Press, pp. 653-686.

[5] Papadioti I., Danas K. and N. Aravas N. (2016), "A methodology for the estimation of the effective yield function of isotropic composites", Int. J. Solids Struct. Vol. 87, pp. 120-138.

[6] Kaufman E.H., Jr., Leeming D.J. and Taylor G.D. (1995), "An ODE-based approach to non-linearly constrained minimax problems", Numerical Algorithms Vol. 9, pp. 25-37.

[7] Papadioti I. (2016), "Non-linear Homogenization Theories with Applications to TRIP Steels. Ph.D. Thesis. University of Thessaly, Greece.

[8] Segurado J. and Llorca J. (2002), "A numerical approximation to the elastic properties of sphere-reinforced composites", J. Mech. Phys. Solids, Vol. 50, pp. 2107-2121.

[9] Lopez-Pamies O., Goudarzi T. and Danas K. (2013), "The non-linear elastic response of suspensions of rigid inclusions in rubber. II. A simple explicit approximation for finite-concentration suspensions", J. Mech. Phys. Solids Vol. 61, 19-37.

[10] Rintoul M.D. and Torquato S. (1997), "Reconstruction of the structure of despersions", J. Collois Inter. Sci. Vol. 186, pp. 467-476.

[11] Suquet P. and Castañeda P. (1993), "Small-contrast perturbation expansions for the effective properties of non-linear composites", C. R. Acad. Sci. Paris (Série II) Vol. 317, pp. 1515-1522.

[12] Ponte Castañeda P. and Suquet P. (1995), "On the effective mechanical behavior of weakly inhomogeneous non-linear materials", Eur. J. Mech. A/Solids Vol. 14, pp. 205-236.

[13] Idiart M. (2008), "Modeling the macroscopic behavior of two-phase non-linear composites by in finite rank laminates", J. Mech. Phys. Solids Vol. 56, pp. 2599-2617.

[14] Marciniak Z. and Kuczynski K. (1967), "Limit strains in the process of stretch forming sheet metal", Int. J. Mech. Sciences Vol. 9, pp. 609–620.

[15] Papatriantafillou I., Agoras M., Aravas N. and Haidemenopoulos G. (2006), "Constitutive modeling and finite element methods for TRIP steels", Comp. Methods Appl. Mech. Eng. Vol. 195, pp. 5094–5114.